Electron-Scattering Studies on Ca^{40} and Ca^{48}†

R. A. EISENSTEIN,* D. W. MADSEN, H. THEISSEN, L. S. CARDMAN, AND C. K. BOCKELMAN
Electron Accelerator Laboratory, Yale University, New Haven, Connecticut 06520

(Received 19 June 1969)

The beam from the Yale University Electron Accelerator has been used in systematic studies of the nuclear charge distributions of Ca^{40} and Ca^{48}. The beam energy has been varied between 20 and 60 MeV, and the angular distributions include angles between 70° and 150°. Elastic electron scattering has been used to obtain the rms radius of Ca^{40}, and a value for the difference between the Ca^{40} and Ca^{48} radii. The results indicate that this difference is not as large as that predicted by the $A^{1/3}$ rule, in agreement with the Stanford electron scattering work and the Chicago and CERN experiments on the spectra from muonic atoms. Inelastic scattering experiments also have been performed, yielding results for the reduced transition probability $B(EL\uparrow)$ and the transition radius R_{tr} for the following states: Ca^{40}, 3.73-MeV (3−), 3.90(2+), 6.94(2+, 3−); Ca^{48}, 3.83-MeV (2+) and 4.51-MeV (3−).

I. INTRODUCTION

THE Ca isotopes have been the subjects of much experimental[1–7] and theoretical[8–10] interest. This is in large part due to the fact that Ca^{40} and Ca^{48}, which occupy the ends of the stable isotope series for this element, are both doubly magic nuclei within shell-model theory. For this reason, knowledge concerning the structure of the ground- and excited-state charge distributions of these two isotopes is of particular value in elucidating the general systematics of nuclei in this region.

Exhaustive experimental investigations into the details of isotopic differences in the ground-state charge distributions of the Ca isotopes have been reported. Frosch[1] and his collaborators at Stanford, using high-energy electron scattering, have found rather sharp negative deviations from the $A^{1/3}$ law as neutron numbers increase. The effect becomes most pronounced at Ca^{48}, where the experiments indicate that ${}_{48}R_m < {}_{40}R_m$, R_m being the rms radius of the nuclide. General agreement with these findings has been obtained in the observation of the muonic x-ray spectra of the Ca isotopes in careful experiments by Ehrlich[2] and co-workers at Chicago. Acker *et al.*[3] at CERN have studied muonic x rays from Ca^{40}.

It is, however, important to realize that these two experimental methods are not measuring the same physical quantity. The muonic x-ray experiment in lighter nuclei like Ca^{40} measures the rms value of the ground-state charge distribution R_m, although model dependence does enter slightly. High-energy electron-scattering measurements cannot measure R_m directly, because the cross section becomes sensitive to higher moments to such an extent that the final results are significantly model-dependent. Several charge distributions may yield excellent agreement with the experimental form factor, but give different R_m values. Since the models used are phenomenological to start with, the parameters related to nuclear size can be extracted from the data only within the confines of a particular nuclear model. This is not to minimize the fact that these measurements are accurate indicators of the shape and finer details of the charge distribution, and have severely limited the class of acceptable models. The point is rather that information from several different experiments is often needed to form a unified whole. Ultimately, any complete description of charge structures must not only give the correct R_m, but also the correct form factor at high values of the momentum transfer q.

The low-q electron-scattering experiment reported here seems a natural bridge between the muonic work and the high-q scattering experiments, because it too provides an almost model-independent method of extracting rms radii. Because size effects are small at low q, the experiment has centered about Ca^{40} and Ca^{48} since the effect is largest between these two nuclei. Its aim has been to extract model-independent values for ${}_{40}R_m$ and for the difference in rms radii between Ca^{40} and Ca^{48}.

It has been shown in earlier work[11–14] that inelastic

† Work supported by the U.S. Atomic Energy Commission, under Contract No. AT(30-1)2726 with Yale University.

* Present address: Department of Physics, Weizmann Institute of Science, Rehovot, Israel.

[1] R. F. Frosch, R. Hofstadter, J. S. McCarthy, G. K. Nöldeke, K. J. van Oostrum, M. R. Yearian, B. C. Clark, R. Herman, and D. G. Ravenhall, Phys. Rev. **174**, 1380 (1968).

[2] R. D. Ehrlich, D. Fryberger, D. A. Jensen, C. Nissim-Sabat, R. J. Powers, V. L. Telegdi, and C. K. Hargrove, Phys. Rev. Letters **18**, 959 (1967); **19**, 344 (1967); R. D. Ehrlich, Phys. Rev. **173**, 1088 (1968).

[3] H. L. Acker, G. Backenstoss, C. Daum, J. C. Sens, and S. A. DeWit, Nucl. Phys. **87**, 1 (1966).

[4] E. P. Lippincott and A. M. Bernstein, Phys. Rev. **163**, 1170 (1967).

[5] M. A. Grace and A. R. Poletti, Nucl. Phys. **78**, 273 (1966).

[6] A. Marinov and J. R. Erskine, Phys. Rev. **147**, 826 (1966).

[7] R. J. Peterson, Phys. Rev. **140**, B1479 (1965).

[8] W. J. Gerace and A. M. Green, Nucl. Phys. **A93**, 110 (1967); **A113**, 641 (1968); **A123**, 241 (1969).

[9] G. Bertsch, Nucl. Phys. **89**, 673 (1966).

[10] V. Gillet and E. Sanderson, Nucl. Phys. **54**, 472 (1967).

[11] M. A. Duguay, C. K. Bockelman, T. H. Curtis, and R. A. Eisenstein, Phys. Rev. **163**, 1259 (1967).

[12] J. F. Ziegler and G. A. Peterson, Phys. Rev. **165**, 1337 (1968).

[13] G. A. Peterson and J. Alster, Phys. Rev. **166**, 1136 (1968).

[14] G. Fricke, G. R. Bishop, and D. B. Isabelle, Nucl. Phys. **67**, 187 (1965); F. Gudden and P. Strehl, Z. Physik **185**, 111 (1965); E. Spamer, *ibid.* **191**, 24 (1966); E. Spamer and H. Artus, *ibid.* **198**, 445 (1967).

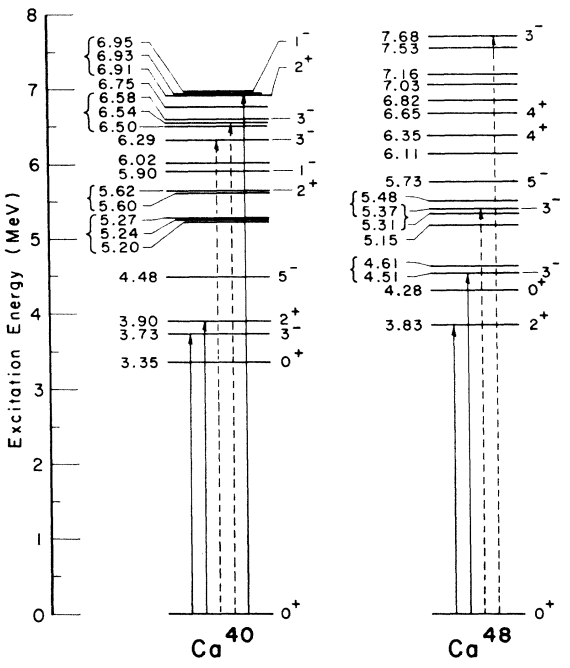

FIG. 1. States of Ca^{40} and Ca^{48}. Solid arrows denote transitions for which form factors are obtained in this work; dashed arrows denote observed transitions for which no form factors have been obtained. Brackets group levels which were not resolved.

electron scattering is a useful tool for the investigation of the electromagnetic properties of excited nuclear states. In particular, values of the reduced transition probability $B(EL\uparrow)$ and the so-called transition radius R_{tr} can be reliably extracted from the experimental inelastic form factors. These quantities are, in principle, just as useful in mapping out the charge structure of the excited states as Z^2 and R_m are in the case of the ground states. The intent of this part of the experiment is to obtain transition rates and R_{tr}^2 values for several states of interest in Ca^{40} and Ca^{48}. Figure 1 shows the level diagrams for these nuclei and the levels studied in this work. These include the first 2+ and 3− states of the two isotopes.

In addition, a triplet of states at 6.94 MeV has been investigated in Ca^{40}, and $B(EL\uparrow)$ values are reported for the 2+ and 3− states in this group. Several weaker transitions in both isotopes have been observed, but are too weak to obtain information on anything but their relative strengths. All of these results are compared with other recent experimental and theoretical findings.

II. EXPERIMENTAL DETAILS

All of the measurements reported in this work were performed on the Yale Electron Accelerator. This machine, as well as all of the electron scattering apparatus, has been described in previous papers[11,12] and theses.[15–17] For these experiments, energies between 20 and 60 MeV were used, in conjunction with scattering angles that varied from 70° to 150°. The corresponding momentum transfer q hence varied from 0.1 to 0.6 F^{-1}. Total energy resolution was 0.27%. A four-channel detector ladder was used to collect the data.

Targets of graphite, Ca^{40}, and Ca^{48} were used in the experiment. The C^{12} and Ca^{40} targets were manufactured in our laboratory from a pressed carbon rod and a bar of natural Ca (97.0% Ca^{40}). To avoid oxygen contamination the Ca target was prepared in an oil bath, then cleaned and kept under vacuum at all times. The Ca^{48} target was obtained on a loan agreement from the U.S. Atomic Energy Commission.[18] The target thicknesses and major impurities are shown in Table I. The information on the Ca^{48} target comes a mass analysis performed at Oak Ridge.

Target thicknesses were calculated by dividing weight by area. To measure the area each target was placed in an airtight plastic container together with a square brass piece of very accurately known surface area. The container was then placed in a photographic enlarger, and a shadow photograph was taken of both objects. To avoid systematic errors, the areas were about 25 times enlarged, both on the same sheet of paper, which was dimensionally stable under development (Kodak Resisto-Rapid). The areas of the dried pictures were measured with a planimeter, and the area of the target found by normalizing the area of its picture to that of the square. Targets were held flat, and the brass square had bevelled edges in order to prevent parallax. Attempts were made to avoid errors due to aberrations in the enlarger lenses.

The target thickness thus measured are values averaged over the entire target. During manufacture, attempts were made to keep the thickness uniform over the whole surface; this was checked using a

TABLE I. Information concerning the targets used in this experiment.

Isotope	Purity	Major impurity	Thickness (mg/cm²)	Fractional radiation length
C^{12}	98.9%	C^{13}, 1.1%	70.7±0.3	1.6×10^{-3}
Ca^{40}	97.0%	Ca^{44}, 3%	28.8±0.2	1.8×10^{-3}
Ca^{48}	96.3%	Ca^{40}, 3.6%	25.8±0.2	1.3×10^{-3}

[15] Michel A. Duguay, Ph.D. thesis, Yale University, 1966 (unpublished).
[16] T. H. Curtis, Ph.D. thesis, Yale University, 1968 (unpublished).
[17] R. A. Eisenstein, Ph.D. thesis, Yale University, 1968 (unpublished).
[18] Through the Isotope Sales Division of the Oak Ridge National Laboratory.

TABLE II. Experimental data and best theoretical fit for the Ca^{40}-C^{12} measurements. The percent error includes only the experimental uncertainties, part of which is a 1.5% systematic error. Errors due to uncertainties in the C^{12} cross section are not included. Theoretical values of the C^{12} cross section are calculated using the charge distribution of Eq. (2).

Lab angle (deg)	Experimental ratio $R_{40}^{expt}=\sigma(40)/\sigma(12)$	% error	Best-fit ratio $R_{40}'=\sigma(40)/\sigma(12)$	Theoretical C^{12} cross section (F^2/sr)
Incident energy = 43.24 MeV				
70.17	10.82	2.3	10.64	0.5619×10^{-1}
90.07	10.30	2.4	9.839	0.1717×10^{-1}
110.07	9.23	2.3	9.097	0.5854×10^{-2}
130.06	8.50	2.4	8.412	0.2004×10^{-2}
150.14	8.10	2.3	7.912	0.5555×10^{-3}
Incident energy = 60.21 MeV				
70.17	8.57	2.4	9.036	0.2554×10^{-1}
90.07	7.33	2.4	7.691	0.7308×10^{-2}
130.06	5.26	2.3	5.338	0.7526×10^{-3}
150.14	4.63	2.5	4.632	0.1997×10^{-3}

micrometer. As a further safeguard, the targets were placed off-center in the beam and continually rotated to average out nonuniformities.

In order to protect the targets from oxidation or other contaminants, a special chamber[17] was constructed to serve both as a target chamber and storage container. It can be converted from one use to the other, maintaining a vacuum at all times.

III. ELASTIC SCATTERING FROM Ca^{40}

The first goal was to determine the rms radius of Ca^{40} (hereafter called ${}_{40}R_m$). This was done by measuring the ratio of the Ca^{40} cross section to that of C^{12}. The choice of C^{12} instead of the proton as a comparison nucleus was possible because its cross section, relative to that of the proton, is now well known.[19] This offers an experimental advantage, since C^{12} targets are much easier to handle than hydrogen-containing targets. The cross sections were measured under constant experimental conditions, in rapid succession, in order to eliminate a number of systematic errors.

A. Experimental Ratios

The experimental ratios were calculated from the following equation:

$$R_{40}^{expt}=\frac{\sigma_e(Ca^{40})}{\sigma_e(C^{12})}=\frac{(SKA/d)_{Ca^{40}}}{(SKA/d)_{C^{12}}}. \quad (1)$$

Here S is the area under the elastic peak, corrected for background, dead time, and spectrometer dispersion; K is a radiation correction factor to be described; A is the atomic weight ($A=40.08$ for Ca^{40}, 12.01 for C^{12}); d is the target thickness. The background was measured without a target in place, all other conditions being equal, and led to a small (<1%) correction in all cases. The dead-time correction was less than 4% in all cases, and less than 2% in most.

The correction factor K takes into account the usual radiative processes: the production of real and virtual photons[20] during the scattering event (the Schwinger correction) and the production of bremsstrahlung[21] by the electrons passing through the target. In order to minimize errors in the radiative corrections, the elastic peak area was integrated out to 1.5 MeV below the peak center in all cases. K also includes a small correction[22] (<0.3%) arising from ionization losses in the target (Landau correction). Contributions of Ca isotopes other than Ca^{40} were taken into account as described in Sec. IV A below.

B. Errors

The statistical error in counting was on the order of 0.5%. The determination of the target thicknesses as described in Sec. II involved the use of a planimeter, the readings of which scattered with an rms deviation of 0.5%. The error in the C^{12} cross section (2%) is essentially statistical.[19] Its effect on the Ca^{40} measurement is discussed below. Errors in the energy calibration (0.3%), in the angle calibration (0.2%), and in the charge collection efficiency (0.1%) were treated as statistical errors and added quadratically. Systematic errors, the largest source of which was in the target thickness determination, were added linearly, and led to an estimate of 1.5% systematic error in R_{40}^{expt}.

[19] R. Engfer and D. Türck, Z. Physik **205**, 90 (1967).

[20] J. W. Motz, Haakon Olsen, and H. W. Koch, Rev. Mod. Phys. **36**, 881 (1964).

[21] H. Crannell, Phys. Rev. **148**, 1107 (1966).

[22] H. Breuer, Nucl. Instr. Methods **33**, 226 (1965).

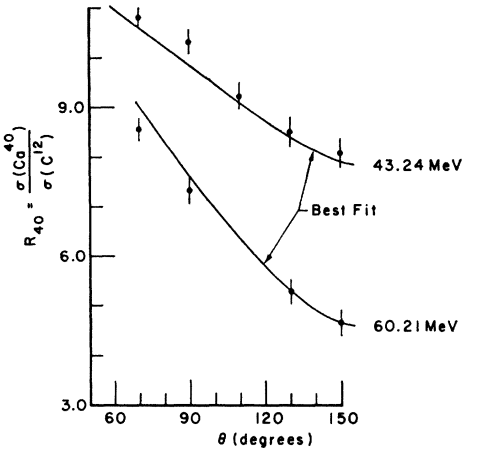

FIG. 2. Experimental results for the Ca^{40}-C^{12} cross-section ratios. The solid line is the best theoretical fit, with $c=3.650$ F, $t=2.280$ F for Ca^{40}, and ${}_{40}R_m=3.423$ F. Error bars include both experimental error (systematic and statistical) and the error of analysis, which includes the error in the C^{12} comparison cross section because of the uncertainty of ${}_{12}R_m$. See text.

C. Analysis

In all, nine data points were taken, five at 43.24 MeV and four at 60.21 MeV. These are given in Table II, along with the experimental error in each point. Also shown are the theoretical ratios $R_{40}{}^t$ which best fit the data. These were calculated using the phase-shift computer code of Rawitscher and Fischer,[23] modified to accept any one of several nuclear models. The results from this code were checked against published results[24] of a code by Bühring and found to agree within 0.2% between 30° and 155°. All cross sections were calculated in the center-of-mass system and converted[25] to the lab reference frame.

The charge-distribution parameters for C^{12} used in this work were taken from the work of Engfer and Türck,[19] who with the assumption of the usual shell-model distribution for $1s$ and $1p$ protons,

$$\rho(r)=[1+\alpha(r/a)^2]\exp[-(r/a)^2], \qquad (2)$$

obtained $a=1.669$ F and $\alpha=1.006$. These values lead to an rms radius value for C^{12} of ${}_{12}R_m=2.42\pm0.04$ F, which is model-independent.

The Ca^{40} trial cross sections were computed using at first a Fermi distribution

$$\rho(r)=\rho_0\{1+\exp[(r-c)/a]\}^{-1}, \qquad (3)$$

and varying the parameters c and a until a best fit was obtained for the cross-section ratio R. The best fit was determined by minimizing the conventional χ^2 quantity:

$$\chi^2=\sum_{i=1}^{M}\frac{(R_i{}^t-R_i{}^{\text{expt}})^2}{(\delta R_i{}^{\text{expt}})^2}. \qquad (4)$$

The sum is over the M sets of experimental conditions (nine in this case); $R_i{}^t$ is the theoretical prediction for experimental conditions i; $\delta R_i{}^{\text{expt}}$ is the absolute statistical uncertainty in $R_i{}^{\text{expt}}$. Here a distinction must be drawn between purely experimental errors and those introduced by a particular means of data analysis. The experimental errors are obtained as described in Sec. III B. When extracting the value of ${}_{40}R_m$ from the data, however, knowledge of the comparison C^{12} cross section is required. The error in this cross section depends on the error in the C^{12} rms radius, and further, it will increase with q as ${}_{12}R_m$ becomes more important. This source of error is included in the denominator of Eq. (4) as a statistical error, since the uncertainty in ${}_{12}R_m$ is statistical.[19] In this way, the fit (and also ${}_{40}R_m$) is conditioned by the precision with which ${}_{12}R_m$ is known.

The minimum occurred for $c=3.650$ F and $t=2.280$ F with t the skin thickness, defined as the distance over which $\rho(r)$ changes from 90 to 10% of its maximum value. Here and elsewhere in this paper, the approximation $t=4a\ln 3$ is used; it is accurate to within 0.5%. At the minimum, $\chi^2/N=5.8$ ($N=M-2$). Figure 2 shows the experimental points and the lines of best fit, generated by the Rawitscher-Fisher code with the above charge distributions. The errors shown include the experimental errors of Table II and the error introduced by the analysis, as mentioned above.

The rms radius R_m can be calculated from any pair (c, a) using the relation (for $a\ll c$)

$$R_m{}^2=\tfrac{3}{5}c^2[1+(7/3)(\pi^2a^2/c^2)]. \qquad (5)$$

For the above (c, a) pair, $R_m=3.423$ F is obtained. For this R_m value several other (c, a) pairs were tried. Except at extreme (c, a) values, all gave a comparable χ^2. This demonstrates that only one shape parameter, here taken to be the rms radius, can be extracted uniquely from low-energy electron-scattering data. There is, of course, a slight dependence of the rms radius on the actual choice of charge-distribution parameters. In order to investigate this quantitatively, a value of t was fixed and a best fit to the data ob-

TABLE III. Range of Fermi distribution charge parameters which give statistically equivalent fits to the Ca^{40} elastic scattering cross sections.

Fixed t (F)	Best-fit c (F)	Implied R_m (F)
1.980	3.823	3.402
2.270	3.650	3.417
2.475	3.510	3.432
2.996	3.030	3.455

[23] G. H. Rawitscher and C. R. Fischer, Phys. Rev. **122**, 1330 (1961); C. R. Fischer and G. H. Rawitscher, *ibid.* **135**, B377 (1964).

[24] H. A. Bentz, R. Engfer, and W. Bühring, Nucl. Phys. **A101**, 527 (1967); W. Bühring, Z. Physik **192**, 13 (1966).

[25] L. L. Foldy, K. W. Ford, and D. R. Yennie, Phys. Rev. **113**, 1147 (1959).

tained by varying c. A series of such fits were sought for fixed values of t between 2 and 3 F. The corresponding values of c and R_m are listed in Table III. It is important to note that these fits were essentially equivalent in quality, in that χ^2/N did not vary significantly from 5.8. Table III shows that while t varied by 50%, R_m changed by only 2%. This variation may be ascribed to the influence of higher moments of the charge distribution on the cross section.

The effect of higher moments can also be studied by using different models for the charge distribution. This was done using equivalent fitting procedures. The models include the square well,

$$\begin{aligned} \rho(r) &= 3/4\pi R^3 \qquad (0<r\leq R) \\ &= 0, \qquad\qquad (r>R) \\ R_m^2 &= \tfrac{3}{5}R^2, \end{aligned} \tag{6}$$

the three-parameter wine-bottle shape,[1]

$$\rho(r) = [1+w(r/c)^2]\{1+\exp[(r-c)/z]\}^{-1}, \tag{7}$$

and a harmonic-well model,

$$\begin{aligned} &\rho(r) = N_0[1+\alpha y^2+(R\alpha/5)y^4]\exp(-y^2), \\ &R_m^2 = \tfrac{3}{2}b^2[(1+2R)/(1+R)]. \end{aligned} \tag{8}$$

The harmonic-well shape was derived for Ca^{40} by assuming that the nuclear protons obey the extreme single-particle shell model. Harmonic-oscillator wave functions have been used for the radial parts of the wave functions. The parameters in the above distribution are given by

$$y=r/b, \qquad b^2=a^2+a_p^2, \qquad R=a/a_p,$$
$$\alpha = R/(1+\tfrac{1}{2}R+\tfrac{1}{4}R).$$

The quantity[26] a_p ($\sim$0.85 F) is a parameter related to the charge distribution of the proton, which was folded into the strict shell-model distribution. Hence, a is the only free parameter and it corresponds to the oscillator parameter chosen for the protons. However, two parameters have been used to fit the data, R and b.

The shapes of best fit for all these distributions are shown in Fig. 3, along with the equivalent R_m values. With the exception of the square well, all values of R_m are within 1% of that obtained using the Fermi distribution. It should be emphasized that on the basis of this experiment, all these models are equivalent since they cannot be distinguished within the experimental error. Of course, the Stanford experiments have limited the acceptable models to the Fermi and wine-bottle shapes.

The present result can be viewed in conjunction with the high-energy results obtained at Stanford to obtain more information. Work by Croissiaux[27] and collaborators has indicated that a t value near 2.50 F for the Fermi distribution is appropriate to Ca^{40}. Specializing to a value of 2.475 F gives $_{40}R_m=3.432$ F, in excellent agreement with the muonic results of Acker[3] and co-workers which give $_{40}R_m=3.467$ F.

Assuming that the Fermi distribution adequately fits our data we now seek to determine the error associated with R_m. For the case of pure statistical

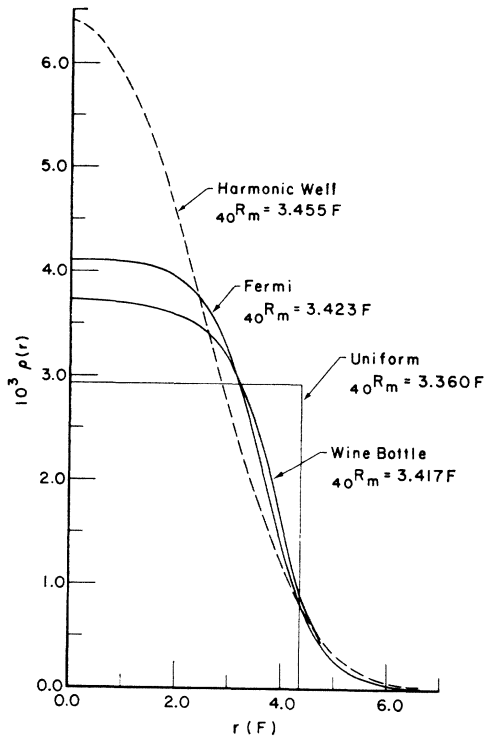

FIG. 3. Graphical representation of various charge distributions assumed for Ca^{40} in analysis. These are best fits for each type shown. Note that all rms radii are nearly identical. All shapes give equally good fits to the data.

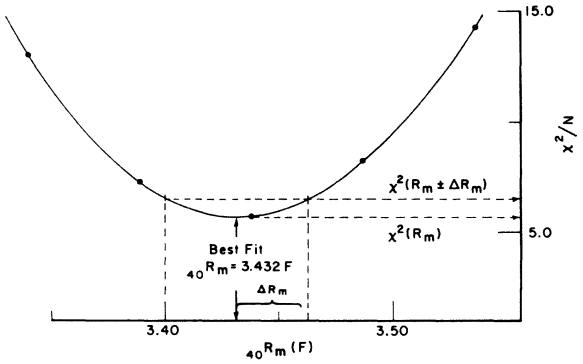

FIG. 4. Determination of standard deviation in $_{40}R_m$ using Eq. (9). Holding t constant at 2.475 F, $_{40}R_m$ was varied and χ^2 obtained. The solid dots are five such points; the solid line is an eye fit to them. The minimum is at $_{40}R_m=3.432$ F; ΔR_m denotes the statistical uncertainty in $_{40}R_m$ from Eq. (9).

[26] T. Janssens, R. Hofstadter, E. B. Hughes, and M. R. Yearian, Phys. Rev. **142**, 922 (1966).

[27] M. Croissiaux, R. Hofstadter, A. E. Walker, M. R. Yearian, D. G. Ravenhall, B. C. Clark, and R. Herman, Phys. Rev. **137**, B865 (1965).

error only, the uncertainty in R_m was deduced from the following[28] formula:

$$\chi^2(R_m \pm \Delta R_m) = \chi^2(R_m)[1+(N-1)^{-1}]. \quad (9)$$

Here N is the number of degrees of freedom. If χ^2 is plotted against R_m, the minimum χ^2 corresponds to the R_m value of best fit. The change in R_m that brings χ^2 to $[1+(N-1)^{-1}]$ of the lowest value is the standard deviation of R_m. Since χ^2 is not constant for all (c, t) pairs corresponding to a particular R_m, the different R_m values were all obtained holding t at 2.475 F and varying c. The results are shown in Fig. 4. The resulting standard deviation is seen to be 0.03 F.

The uncertainty in R_m due to systematic error was calculated in the following way: To each experimental ratio point was added and subtracted the systematic error of 1.5% and new fits made to this data. The difference between this new R_m value and the old was taken to be the systematic uncertainty. For the Ca^{40} measurements, it is 0.04 F; adding the systematic and statistical deviations makes the final result ${}_{40}R_m = 3.43 \pm 0.07$ F.

IV. ELASTIC SCATTERING FROM Ca^{48}

The Ca^{48} measurements were carried out using the same general methods as in the Ca^{40} case. Here, however, the Ca^{48} cross section was measured relative to Ca^{40} rather than C^{12}. This has a distinct advantage in that the observed ratio $\sigma(48)/\sigma(40)$ (hereafter called R_{48}^{expt}) will reflect directly the differences in the rms radii, and will be to a large degree insensitive to the exact R_m value used for Ca^{40} in the analysis. The fact that both nuclei are isotopes of the same element ensures, furthermore, that the radiative corrections to the cross sections will largely cancel out of the ratio R_{48}^{expt}.

Before going into the details of the data analysis, a brief examination of the major features of electron scattering from the standpoint of the Born approximation is helpful. All of the essentials are preserved, even though the final results are not of sufficient accuracy to allow them to be used in analysis of the data. There, one must resort to the full distorted partial-wave treatments.

In the case of low-q elastic scattering the differential cross section in Born approximation is

$$\sigma_e(q \to 0) = \sigma_{\text{Mott}}[1-(q^2/3)R_m^2]$$

with

$$\sigma_{\text{Mott}} = (Ze^2/2E)^2 \cos^2(\tfrac{1}{2}\theta)/\sin^4(\tfrac{1}{2}\theta);$$

E is the incident electron energy, θ is the scattering angle; nuclear recoil is neglected. The quantity

$$R_{48} = \sigma_e(Ca^{48})/\sigma_e(Ca^{40}) = 1-\tfrac{1}{3}q^2({}_{48}R_m^2 - {}_{40}R_m^2)$$

is expected to approach unity as $q \to 0$, and will have a nonzero slope if one of the nuclei has a bigger rms radius. Hence, an indication of relative size can be obtained independent of any model just from the experimental ratios of the cross sections.

A. Experimental Ratios

Data were taken at three energies for this part of the experiment. Data at 21.49 MeV were obtained for the purpose of checking the relative thicknesses of the two targets in a way independent of the mechanically measured values previously quoted, and will be discussed later. Sets of data at 40.64 and 60.17 MeV were each taken in one run after long warm-up times to stabilize the analyzer. Two additional data points were taken at 60.17 MeV and 150° in a later run as a check.

The ratios were computed using Eq. (1), *mutatis mutandis*. The effects of the admixture of Ca isotopes, other than the ones under study, were calculated using the known isotopic contents of natural Ca in the case of Ca^{40}, and the results of spectroscopic analysis by Oak Ridge in the case of Ca^{48}. Isotopes other than those of Ca were of insignificant quantity. Corrections for the Ca isotopes (mostly for Ca^{40} and Ca^{44}) were made using the charge parameters of Frosch *et al.*[1] In addition, the extent of carbon and oxygen contamination was estimated by looking for elastic scattering from these elements at backward angles where recoil will separate their contributions. The total effect on the ratio from these isotopic and

TABLE IV. Experimental data for the Ca^{48}-Ca^{40} measurement, renormalized so that the average ratio at 21.49 MeV is 1.0. The error estimate includes 1.5% systematic error.

Lab angle (deg)	Experimental ratio $R_{48}^{\text{expt}} = \sigma(48)/\sigma(40)$	% error	Theoretical $\sigma(Ca^{40})$ (F^2/sr)
Incident energy = 21.49 MeV			
70.17	0.981	2.3	3.079
70.17	1.020	2.4	3.079
Incident energy = 40.64 MeV			
70.17	1.059	2.4	0.6983
90.07	1.030	2.4	0.2008
110.07	1.022	2.3	0.6447×10^{-1}
130.06	0.998	2.4	0.2079×10^{-1}
150.14	0.994	2.3	0.5512×10^{-2}
Incident energy = 60.17 MeV			
70.17	1.054	2.4	0.2293
90.07	0.992	2.5	0.5524×10^{-1}
110.07	1.007	2.4	0.1471×10^{-1}
130.06	0.997	2.5	0.3990×10^{-2}
150.14	0.950	2.6	0.9209×10^{-3}
150.14	1.018	2.4	0.9209×10^{-3}
150.14	1.004	2.4	0.9209×10^{-3}

[28] R. Engfer, Z. Physik **192**, 29 (1966).

chemical impurities was less than 0.5% and has been taken into account in obtaining the cross sections.

The sources and magnitudes of the statistical uncertainties are the same as in the experiment on Ca^{40}. Here, however, an independent check of target thickness was made by measuring the elastic cross sections of Ca^{40} and Ca^{48} at 21.49 MeV and 70°, where point-charge scattering is expected to dominate the cross section. Then the actual value of R_m will have little importance and R_{48}^{expt} should equal unity. This conclusion, suggested by the Born-approximation equations above, was verified by a partial-wave calculation. This experiment was done twice, obtaining ratios of 1.004 and 1.043, respectively. The average ratio is 1.020, a value not inconsistent with the estimate of a systematic error of 1.5% in the target thickness measurements. Considering the effect of possible target nonuniformities, it is believed that the low-energy scattering comparison yields the more reliable measure of the target thickness ratio. Accordingly, the data were renormalized, so that the average ratio at 21.49 MeV is unity. The renormalized data are presented in Table IV.

B. Analysis

The data in Table IV is shown graphically in Fig. 5 along with a theoretical prediction (solid line) using the three-parameter wine-bottle shapes with parameters recently determined by Frosch and collaborators.[1] Referring to Eq. (7), these parameters are

Ca^{48}	Ca^{40}
$c=3.7444$ F	$c=3.6758$ F
$z=0.5255$ F	$z=0.5851$ F
$w=-0.03$	$w=-0.1017$
${}_{48}R_m=3.4762$	${}_{40}R_m=3.4869$ F

$$[({}_{48}R_m-{}_{40}R_m)/{}_{40}R_m=-0.3\%].$$

These parameters, however, do not yield the best fit to the data presented here. The Stanford results show that $(t_{48}-t_{40})/t_{40}$ is equal to $-(12.4\pm1)\%$. Hence, in the subsequent extraction of the difference in R_m from our data, this difference in t values is maintained. This means that if the t value used for Ca^{40} is 2.475 F, near to the value of Croissiaux *et al.*,[27] then the value for t_{48} should be 2.19 F. This value for t_{48} is in disagreement with the absolute value given by Frosch *et al.*, which is 2.351 F.

Using $t_{48}=2.19$ F, fits to the ratio data were made by at first holding ${}_{40}R_m$ fixed at 3.45 F (the average between our results and those of Acker and co-workers,[3] for $t_{40}=2.475$ F) and minimizing χ^2 of Eq. (4) by allowing the R_m difference to vary. This means effectively letting only c vary since the t values are constrained by the relation mentioned above. The best-fit theoretical ratios, shown in Fig. 5, occur for

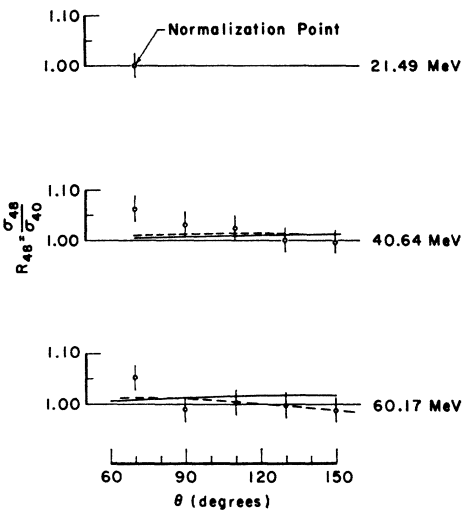

FIG. 5. Experimental ratio data from Table IV. Solid lines are calculated from the parameters of Frosch *et al.*, which imply that $({}_{48}R_m-{}_{40}R_m)/{}_{40}R_m=0.3\%$. Dashed lines show the best fit to the data of this experiment, with the same difference equal to -1%. See text.

a difference in R_m equal to -0.037 F, or -1.1%. The dependence of the R_m difference on the value of ${}_{40}R_m$ was estimated by allowing ${}_{40}R_m$ to vary between 3.35 and 3.50 F. The deviations in the R_m difference from the above quoted value were small compared to the experimental error and therefore are not included in it.

To estimate the statistical error in the R_m difference, Eq. (9) was used. A plot of χ^2 versus R_m difference, similar to Fig. 4, was constructed; from such analysis, the statistical error was found to be $\pm1\%$. The systematic error was found just as in the Ca^{40} case. All ratio data were systematically shifted up and down by $\pm1.5\%$, and new fits made to the data. This resulted in changes of $\pm1\%$ in the value of the R_m difference. Adding the contribution of both these sources of error, the final result of the measurement was taken be $({}_{48}R_m-{}_{40}R_m)/{}_{40}R_m=-(1\pm2)\%$.

Before continuing to a more complete discussion of this result, some specific concerns with the data should be noted. The most obvious is that the 70° data for both 40 and 60 MeV are high, the former by more than two standard deviations. As mentioned earlier, the cross-section ratio, as $q\to0$, should approach unity, signifying the disappearance of finite-size effects in favor of pure-Mott scattering. Target impurities could cause such a disparity, but then it should also appear in the 20-MeV data. As stated earlier, these latter data were taken to measure the effective target thickness, and will include effects of incorrect thickness measurements, as well as those due to impurities. In addition, the known impurities were taken into account. We are not aware of any systematic errors that would tend to raise these 70° points.

Another difficulty is that the over-all trend of the 40-MeV data seems to be of negative slope. This behavior would be expected in the case where ${}_{48}R_m > {}_{40}R_m$ if, in addition, the cross-section ratios were less than unity, and approaching 1 as $q \to 0$. For this data to truly reflect a positive R_m difference of the magnitude (6%) indicated by the slope alone would require an over-all additional renormalization of 8%. In view of our experimental procedure, this seems out of the question.

The trend of the 60-MeV data is satisfactory.

C. Discussion

The elastic scattering measurements described here have obtained a value for the rms radius of Ca^{40} of 3.43 ± 0.07 F. In addition, the fractional difference in rms radii between Ca^{48} and Ca^{40} $({}_{48}R_m - {}_{40}R_m)/{}_{40}R_m$ has been measured to be $-1 \pm 2\%$. This value contrasts sharply with the value of $+6.2\%$ expected on the basis of the $A^{1/3}$ rule. Both of these results are in good agreement with the muonic x-ray experiments conducted at Chicago[2] and CERN,[3] and the high-energy electron-scattering results obtained at Stanford.[1] Our results are parameter- or model-dependent only to a slight extent, on the order of 2%, and then only when the charge parameters are allowed to go to unphysical extremes. When the parameter variation is limited to the range of values observed in other experiments the model dependence is even less. In our final result the skin-thickness parameter t has been restricted to the values set by experiments at Stanford.

In view of this model independence, the only information that can be extracted from our experiment concerns the R_m values. In particular, nothing can be said regarding the isotopic variations of the parameters for any model (apart from R_m) since the parameters are too strongly correlated by R_m. The Stanford experiments, however, have been able to extract these variations[1,27] with considerable success.

The general indication from all of these experiments on relative size is that, from the viewpoint of the shell model, the closure at $N = 28$ is better than that for $N = 20$. Other support for this conjecture comes from the fact that the level structure of Ca^{49} is single-particle in nature, whereas Ca^{41} is much more complex.

Several attempts[29–31] to explain the differences in structure have been made, all of them based on the independent-particle shell model. The calculations start from a Woods-Saxon potential, the half-density radius of which is varied as $A^{1/3}$, while the depth is adjusted to give the correct binding energies. It is known that the proton binding energies for isotopes of the same element increase with neutron excess. One can account for this by introducing an isospin-dependent term in the potential.[30] Because of the increase in binding energy the wave functions of the protons are more and more concentrated towards the center of the nucleus. The calculations show that this effect more than compensates for the $A^{1/3}$ change in the potential radius, thus leading to charge radius differences which are smaller than those predicted by the $A^{1/3}$ rule. It was also shown[31] that the potential parameters compatible with the electron-scattering data are consistent with those needed to fit the separation energies obtained from $(p, 2p)$ and $(e, e'p)$ experiments, as well as with mass differences.

V. INELASTIC SCATTERING

Using the methods described previously[11–17] by several authors, the form factors (at low-momentum transfer) for the electroexcitation of several states (see Fig. 1) in Ca^{40} and Ca^{48} have been obtained. Energies of 41 and 60 MeV have been used, with scattering angles between 70° and 150°, inclusive. This corresponds to momentum transfers $0.32 \leq q \leq 0.57$ F^{-1}. From these form factors, the reduced transition probability $B(EL\uparrow)$ and the "transition radius" R_{tr} have been extracted. Several smaller states were seen in both nuclei, but were not studied in detail.

A. Inelastic Form Factor

Form factors were obtained by measuring the ratio of inelastic to elastic cross section. The following relations hold for the form factors, $|F_{el}|$ for elastic scattering and $|F_{in}|$ for inelastic scattering:

$$|F_{el,in}|^2 \equiv \sigma_{el,in}/\sigma_{Mott},$$
$$|F_{in}|^2 = C\,|F_{el}|^2. \qquad (10)$$

C is the ratio of inelastic to elastic cross section; these are obtained by measuring the areas of peaks corresponding to elastic and inelastic levels. The elastic form factor must be known to use this equation, but if the ground-state parameters are known, $|F_{el}|^2$ can be calculated using the Rawitscher-Fischer code.[23] Sections III and IV have described at length the measurement of the ground-state charge parameters.

The form factor data were then analyzed using theoretical results from the code DUELS,[32] a distorted partial-wave calculation[33] of electroexcitation of nuclei, assuming one-photon exchange. The best-fit theoretical form factors were found by varying the parameters of the transition charge density, ρ_{tr}, taken to be of the form appropriate to a hydrodynamical model.[34]

[29] B. F. Gibson and K. J. Van Oostrum, Nucl. Phys. **A90**, 159 (1967).
[30] F. G. Perey and J. P. Schiffer, Phys. Rev. Letters **17**, 324 (1966).
[31] A. Swift and L. R. B. Elton, Phys. Rev. Letters **17**, 484 (1966).
[32] S. T. Tuan, L. E. Wright, and D. S. Onley, Nucl. Instr. Methods **60**, 70 (1968), and references therein.
[33] J. F. Ziegler, U.S. Atomic Energy Commission Report No. YALE-2726E-49 (unpublished).
[34] L. J. Tassie, Australian J. Phys. **9**, 407 (1956).

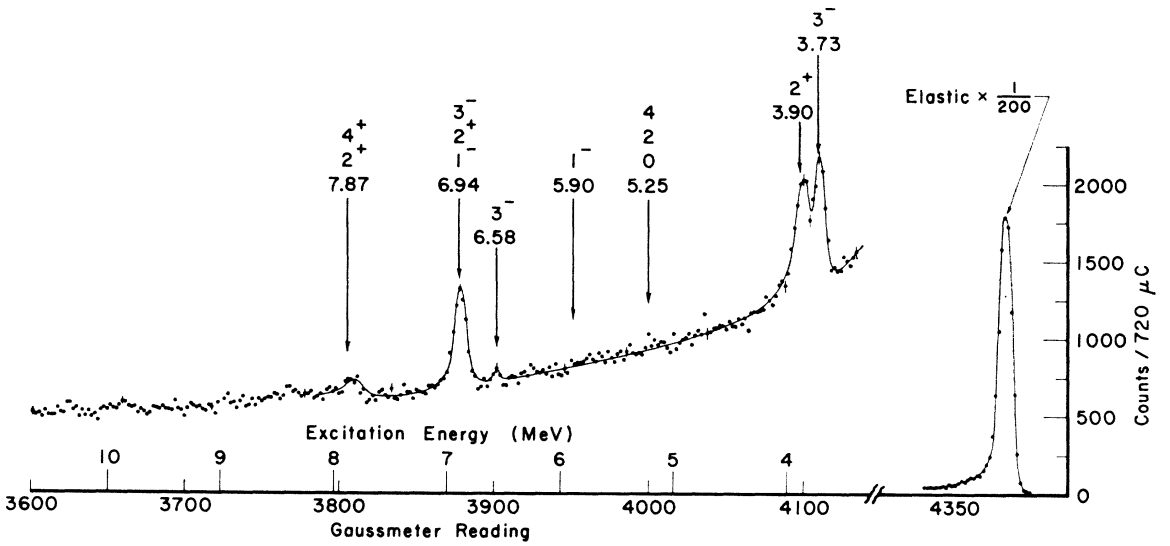

FIG. 6. Spectrum of electrons scattered from natural Ca (97.0% Ca^{40}). The incident energy is 59.87 MeV and $\theta=130°$. Various states of interest are seen, superposed on the radiative tail of the elastic scattering peak. The spectrum has been corrected for background.

The ground-state charge densities (which govern the distortion of the electron waves) are considered fixed by the elastic scattering. Variations of the transition charge densities are expressed in terms of a variation of the quantities $B(EL\uparrow)$ and R_{tr}^2.[11] In low-q Born approximation, these two numbers are sufficient to specify the form factor:

$$|F_{in}|_{q\to 0}^2=\frac{4\pi B(EL\uparrow)}{[(2L+1)!!]^2Z^2}q^{2L}\left(1-\frac{q^2}{2(2L+3)}R_{tr}^2\right)^2.$$

Here only the longitudinal part of the interaction is considered; the transition is $[0^+\to L^\pi,\ \pi=(-)^L]$. Similar behavior has been found in the case of the distorted-wave treatment; when varying the parameters of the transition charge over reasonable excursions, if $B(EL\uparrow)$ and R_{tr}^2 are held constant, the form factor has been found to remain relatively constant also. Further, it is expected that these low-q experiments will not be sensitive to the specific model used for the form of the transition charge. To this extent $B(EL\uparrow)$ and R_{tr}^2 are both parameter- and model-independent.

The quantity $B(EL\uparrow)$ is the usual reduced radiative transition probability,

$$B(EL\uparrow)=(2L+1)\,|\langle f|r^L|i\rangle|^2$$
$$=(2L+1)\left[\int\rho_{tr}^{(L)}(r)r^{L+2}dr\right]^2,$$

while R_{tr}^2 is defined as

$$R_{tr}^2=|\langle f|r^{L+2}|i\rangle|/|\langle f|r^L|i\rangle|$$
$$=\int\rho_{tr}^{(L)}(r)r^{L+4}dr/\int\rho_{tr}^{(L)}(r)r^{L+2}dr.$$

Here $|i\rangle$ and $\langle f|$ refer to the radial parts of the initial and final nuclear wave functions, respectively. Hence, two independent matrix elements involving nuclear states are obtained. Even though we are required to specify these states (through the transition charge) before a distorted-wave calculation can be done, insofar as the calculation is model- or parameter-independent, the best-fit transition charge parameters [or the equivalent $B(EL\uparrow)$ and R_{tr}^2] will be unique within experimental error. The degree of parameter independence of the present results is discussed more fully in Sec. V C.

B. Measurement and Extraction of Form Factors

The experimental $|F_{in}|^2$ values were measured using the same targets as in the elastic scattering case, again rotated to average out thickness fluctuations.

Figures 6 and 7 show spectra of electrons scattered from Ca^{40} and Ca^{48}, respectively, at 60 MeV and 130°. These results were obtained by taking each spectrum in each of three counter telescopes in the detector hodoscope, and combining them into one for the sake of statistics. In practice, the elastic peak was taken first, then the region of interest in the inelastic spectrum, and finally a recheck on the elastic. Energy shifts were entirely negligible, as were efficiency changes in the telescopes. Beam spot position was exceedingly stable, not moving more than 1 diam (1 mm) during any one run.

The radiative tail and inelastic levels can be described by a function of the form[14]

$$N_i=\frac{A}{(\Delta E_i)}+\frac{B}{(\Delta E_i)^2}+\sum_j^{L\text{ peaks}}C_j(E_j)P(E_{el}).\quad(11)$$

The first two terms account for the tail, A and B are variable coefficients, and (ΔE_i) is the energy difference between the elastic peak center and the point i

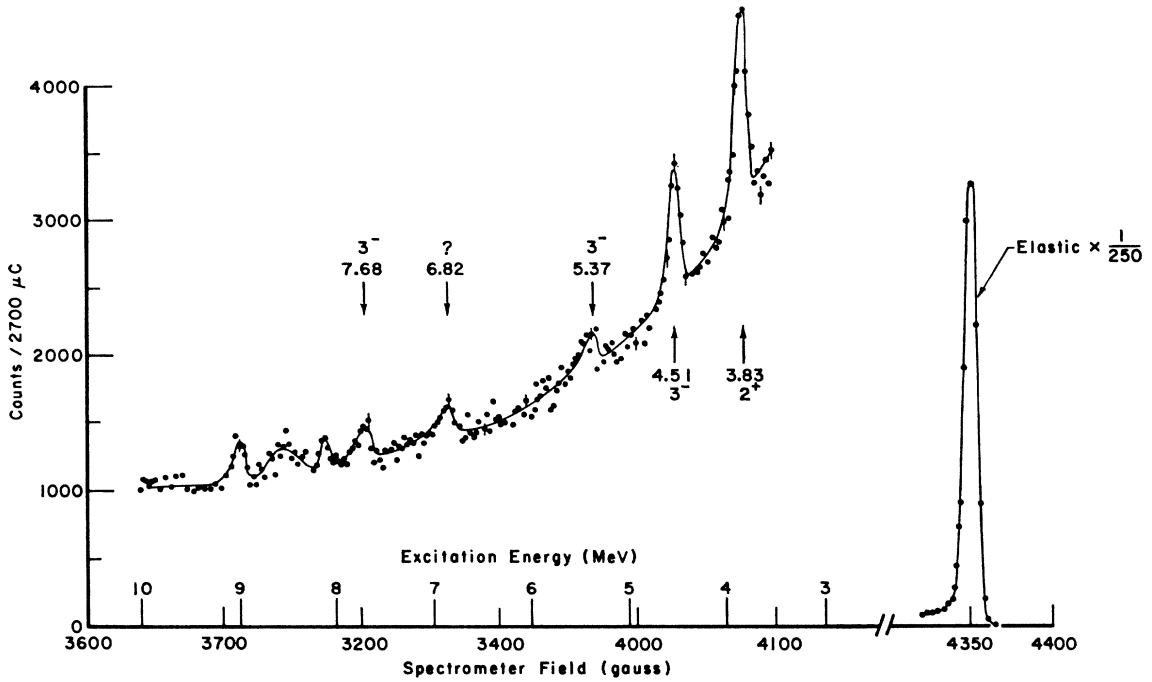

FIG. 7. Spectrum of electrons scattered from Ca^{48}. The incident energy is 60.1 MeV and $\theta=130°$. The spectrum has been corrected for background.

of interest on the tail. The sum is over L inelastic levels; each is assumed to have the same shape as the elastic peak [represented by the known function $P(E_{el})$] differing only by the ratio C_j of inelastic to elastic peak height. This function is fitted to the experimental spectrum, using the method of least squares, and the parameters A, B, and C_j are extracted. The value of C_j is related to the $|F_{in}|^2$ for the particular q in question through Eq. (10).

The inelastic form factors are obtained by multiplying the C_j by the appropriate $|F_{el}|^2$ values for the angle θ and energy E_i. For Ca^{40} the form factors were calculated using $c=3.538$ F and $t=2.475$ F. These values were chosen because the resulting rms radius (3.449 F) is the weighted average between our result and that of Acker *et al.*[3] For Ca^{48}, the rms radius used was 1% smaller (3.412 F) in accordance with our elastic results. The values of c and t were 3.660 and 2.240 F, respectively.

Table V is a compilation of the form factor points obtained for the states of interest. For all but two states, a five-point angular distribution was obtained, using incident energies near 60 MeV. The two exceptions are the 3.83-MeV (2+) state of Ca^{48}, where three additional points were taken (at 41 MeV and 110°, 130°, and 150°) and the 3.73-MeV (3−) state of Ca^{40}, where only four points were obtained. In the analysis each peak has been treated as a single state, although it is clear from Fig. 1 that the 0.27% energy resolution may have included contributions from more than one state in several instances. The special case of the 6.94-MeV peak is discussed in detail later.

The table shows the incident electron energy E_i, the scattering angle θ, and the inelastic momentum transfer

$$q_I \cong (2E_i/\hbar c)(\sin\tfrac{1}{2}\theta)[1-(E_x/E_i)]^{1/2},$$

with E_x the excitation energy of the nucleus. C is the ratio of inelastic to elastic peak heights, obtained from the least-squares fitting routine. $|F_{in}|^2$ is the resulting inelastic form factor from Eq. (10), and the column labeled "% error" is the percent statistical error in the form factor. The column F^* is a restatement of the 41-MeV data; it is this data renormalized to 60.3-MeV incident energy. This is done because code DUELS generates form factors which depend on E_i in addition to q_I. Since this code is expensive to operate, simultaneous fitting of data at several energies becomes prohibitive. The normalization procedure was decided on in the interest of economy and simplicity. The correction is obtained by comparing form factors at the two energies but at the same q_I values. Checks using several sets of parameters showed the corrections to be almost completely model- and parameter-independent. The net result is to lower the inelastic form factors at 41 MeV by 4.5%.

C. Extraction of $B(EL\uparrow)$ and R_{tr}^2

The parameters of the ground-state charge distributions used in code DUELS for the analysis have been stated in Sec. V B. The best fits to the form factors will then yield information[11] regarding the strength and spatial extent of the transition charge density [$B(EL\uparrow)$ and R_{tr}^2, respectively] that is expected to

TABLE V. Experimental form factors for the states of interest in Ca^{40} and Ca^{48}. E_i is the incident electron energy, θ is the scattering angle, q_I is the inelastic momentum transfer, C the ratio of inelastic to elastic peak heights, and $|F_{in}|^2$ the experimental form factor defined by Eq. (10); the sixth column is the percentage error in the experimental form-factor points.

E_i (MeV)	θ (deg)	q_I (F^{-1})	10^4C	$10^3F_{in}^2$	% error	10^3F^{*} [a]
Ca^{40}			3.73 MeV (3−)			
60.36	90.0	0.419	4.62	0.222	6.0	
60.34	110.	0.485	12.91	0.450	2.0	
60.04	130.	0.534	25.30	0.666	2.0	
60.30	150.	0.572	41.90	0.865	6.0	
			3.90 MeV (2+)			
60.50	70.0	0.341	2.24	0.145	6.0	
60.36	90.0	0.419	5.73	0.275	4.0	
60.33	110.	0.485	12.83	0.447	4.0	
60.03	130.	0.533	19.75	0.520	4.0	
60.03	150.	0.571	28.50	0.588	6.0	
			6.94 MeV (2+, 3−)			
60.51	70.0	0.331	1.90	0.123	4.0	
60.36	90.0	0.407	5.71	0.275	2.0	
60.33	110.	0.471	13.00	0.454	2.0	
60.04	130.	0.519	22.65	0.596	2.0	
60.24	150.	0.555	36.02	0.745	2.0	
Ca^{48}			3.83 MeV (2+)			
60.21	70.0	0.339	1.87	0.122	5.0	
60.17	90.0	0.418	6.45	0.311	5.0	
60.15	110.	0.484	11.35	0.399	5.0	
60.13	130.	0.535	19.15	0.502	5.0	
60.18	150.	0.570	26.21	0.546	8.0	
41.07	110.	0.325	2.37	0.165	7.0	0.157
41.05	130.	0.359	2.80	0.173	8.0	0.165
41.07	150.	0.383	3.88	0.219	7.0	0.209
			4.51 MeV (3−)			
60.21	70.0	0.337	0.35	0.0228	17.0	
60.15	90.0	0.415	1.77	0.0854	8.0	
60.15	110.	0.481	5.51	0.194	8.0	
60.14	130.	0.531	12.11	0.317	4.0	
60.18	150.	0.567	21.94	0.456	8.0	

[a] F^{*} denotes the values of $|F_{in}|^2$ at 41 MeV renormalized to 60.2 MeV.

be essentially independent of the particular model used to extract it. A common form for the transition charge density is a shape like a Gaussian or a δ function, peaked at the nuclear surface. This simple picture has been extended by Tassie[34] to form the so-called hydrodynamic model, based on the theory of an incompressible, irrotational liquid drop. He finds, for an excitation of multipole order $L(L\neq 0)$, that

$$\rho_{tr}^{(L)}(r)\sim r^{L-1}[(d/dr)\rho_F(r, c, t)]_{c=c_0, t=t_0},$$

where ρ_F is the ground-state charge distribution, taken here to be of the Fermi shape, with c_0 and t_0 the ground-state parameters. This transition charge density peaks at $r=c_0$.

A deviation from this strict model is obtained by allowing c and t to vary from their ground-state values. For the sake of clarity, the values of c and t will be designated c_{tr} and t_{tr}. Code DUELS makes use of a unrestricted form of the hydrodynamic model which allows for this variation in c_{tr} and t_{tr}.

The experimental data has been fitted (see Ref. 11) to the theoretical form factors using χ^2 as the indicator of best fit [Eq. (4)]. The parameters of the transition charge were varied until minimum χ^2 was obtained, all other parameters being known.

Figures 8–10 show the form factors of best fit for the states under study. The final results for $B(EL\uparrow)$ and R_{tr}^2 are in Table VI along with the c_{tr} and t_{tr} values which gave these results. (Recall that the ground-state parameters c_0 and t_0 are different for the

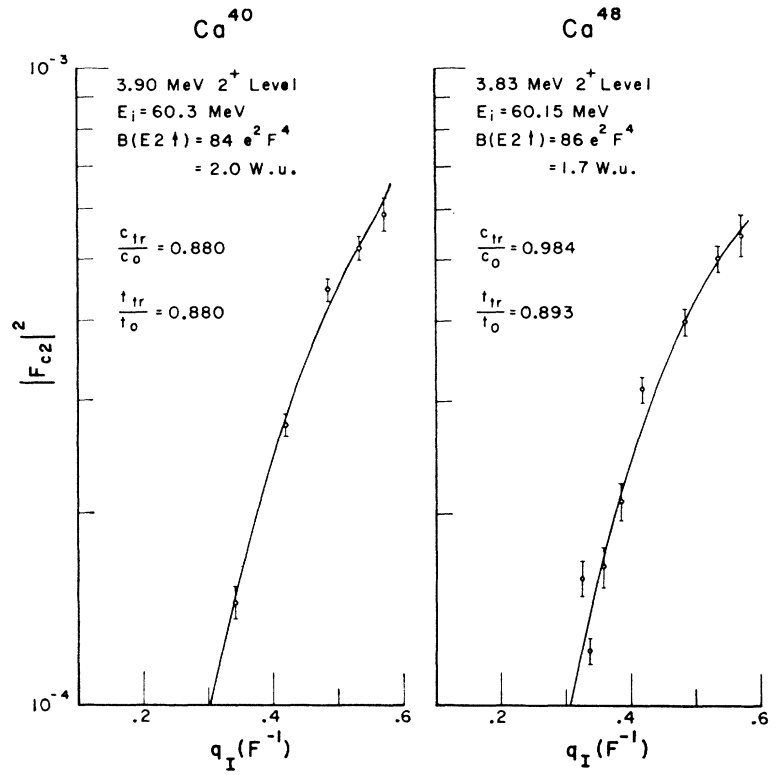

FIG. 8. Experimental form factor points and best theoretical fits to them for the first 2+ states in Ca^{40} and Ca^{48}. The experimental points and their errors are given in Table V.

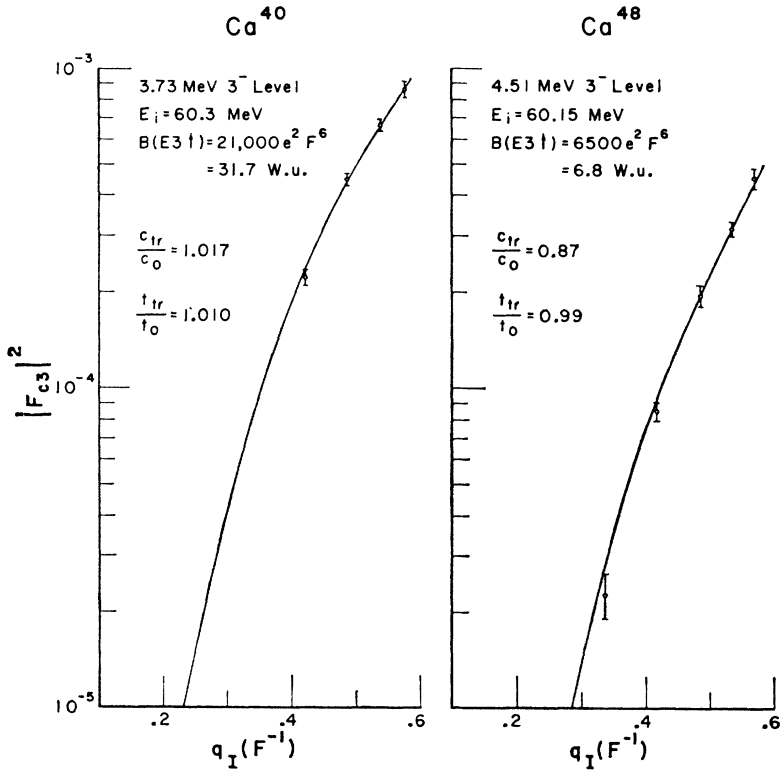

FIG. 9. Experimental form factor points and best theoretical fits to them for the first 3− states in Ca^{40} and Ca^{48}. The experimental values are given in Table V.

TABLE VI. Best-fit values of $B(EL\uparrow)$ and R_{tr}^2 for the states studied in this work. G is the $B(EL\uparrow)$ value expressed in single-particle Weisskopf units. Γ_γ^0 is the partial width for γ decay to the ground state. The column labeled % is the statistical error in $B(EL\uparrow)$. An additional 12% uncertainty must be included in the final error to account for the dependence of $B(EL\uparrow)$ and R_{tr}^2 on the parameters of the transition charge density. N is the number of degrees of freedom in the fit. The transition charge parameters c_{tr} and t_{tr} are given as ratios to the ground-state parameters, which are different for Ca^{40} and Ca^{48}. See the text.

Nucleus	State energy (MeV)	$B(EL)$ (e^2F^{2L})	G (spu)	Γ_γ^0 (eV)	%	χ^2/N	Confidence level (%)	c_{tr}/c_0	t_{tr}/t_0	R_{tr}^2 (F^2)
				2+ States						
Ca^{40}	3.90	84	2.0	1.23×10^{-2}	2	3.5/3	35	0.880	0.880	19.2
Ca^{40}	6.94	70	1.7	1.94×10^{-1}	2	0.5/3	90	1.0	1.0	24.8
Ca^{48}	3.83	86	1.7	1.14×10^{-2}	2	4.5/6	60	0.984	0.893	20.9
				3− States						
Ca^{40}	3.73	21 100	31.7	1.14×10^{-5}	2	0.9/2	65	1.017	1.01	32.3
Ca^{40}	6.94	9 200	13.9	3.83×10^{-4}	3	0.5/3	90	1.00	1.00	31.5
Ca^{48}	4.51	6 500	6.8	1.32×10^{-5}	3	1.5/3	65	0.87	0.99	25.5

two isotopes.) The listed errors in $B(EL\uparrow)$ are statistical only. The χ^2 values for the fits and the number of degrees of freedom N are shown, along with confidence levels obtained from conventional χ^2 tables. N is defined as the number of data points less the number of free parameters, two in this case.

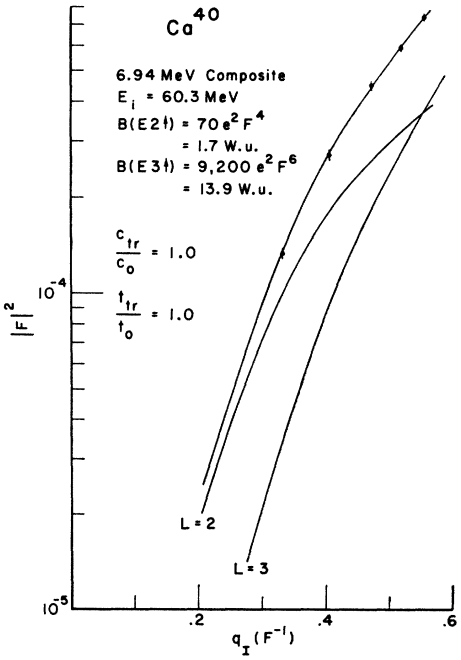

FIG. 10. Experimental points and best theoretical fit to them for the triplet of states near 6.94 MeV. For reasons described in text, only the 2+ and 3− states are assumed to contribute to the cross section. These are accounted for by separate form factors generated within the framework of the strict hydrodynamic model. The $B(EL\uparrow)$ values are varied until best fit is obtained. Neither the 2+ nor the 3− form factor alone will fit the data. Both separate and combined form factors are shown in the figure as solid lines.

The $B(EL\uparrow)$ results are also expressed in terms of their ratio G to the Weisskopf single-particle estimate

$$G=B(EL\uparrow)/B(EL\uparrow)_{sp},$$
$$B(EL\uparrow)_{sp}=[(2L+1)/4\pi]\{[3/(L+3)]R^L\}^2, \quad (12)$$
$$R=1.20A^{1/3},$$

and as a partial width for γ decay to the ground state via the relation

$$\Gamma_\gamma^0=\frac{8\pi\alpha}{[(2L+1)!!]^2}\left(\frac{L+1}{L}\right)\frac{E_x^{2L+1}}{(\hbar c)^{2L}}\left(\frac{2I_g+1}{2I_e+1}\right)B(EL\uparrow).$$

As in the analysis of the elastic scattering, checks were made to ascertain the extent of parameter independence in these results. Two factors enter which make the inelastic case different from the elastic problem.

The first and most obvious is that the scattering depends now on two unknown parameters [$B(EL\uparrow)$ and R_{tr}^2], and not just one (the rms radius R_m), as in the elastic case. Starting with the best fit c_{tr} and t_{tr}, several pairs of parameters were tried, their common feature being that $B(EL\uparrow)$ and R_{tr}^2 were held nearly constant at the best-fit values. The form factors for these pairs gave statistically equivalent fits. In addition, pairs were found that, while giving equivalent fits, allowed $B(EL\uparrow)$ and R_{tr}^2 to vary by as much as 12%. This is in part a reflection of the obvious fact that for a given small number of data points, two free parameters allow greater latitude in fitting than just one. Clearly, the effect of a change in R_{tr}^2 can be compensated to some degree by an appropriate change in $B(EL\uparrow)$. Therefore, to the relatively small statistical error in the fits must be added an additional 12% to account for parameter uncertainty. In the elastic scattering analysis, the Stanford result for t was useful in pinning down the

TABLE VII. $B(EL\uparrow)$ values in Weisskopf single-particle units, Eq. (12), for this and other experiments. See the text for detailed comparison.

Nucleus	Level (MeV)	This work	Doppler shift	Resonance fluorescence	(e, e')	Heavy particle	Theory
			2+ States				
Ca^{40}	3.90	2.0±0.2	1.7±0.4[a] 4.5±1.5[e] 5.7±1.9[h]	···	3.5±1.2[b]	2.9±0.5[c] 3.5±0.7[f]	1.0[d] 1.6[g]
Ca^{40}	6.91	1.7±0.2	···	1.7±0.3[i]	3.9±0.5[b]	···	···
Ca^{48}	3.83	1.7±0.2	···	···	···	5.4±0.8[c]	···
			3− States				
Ca^{40}	3.73	31.7±4	···	···	10.5±3[b]	23.6±3.5[c] 25±4[f]	27[d]
Ca^{40}	6.93	13.8±2	···	···	1.6±0.3[b]	···	3[d]
Ca^{48}	4.51	6.8±1	···	···	···	8.0±1.2[c]	···

[a] Reference 35.
[b] Reference 38.
[c] References 4 and 41.
[d] Reference 8.
[e] Reference 36.
[f] Reference 42.
[g] Reference 9.
[h] Reference 37.
[i] Reference 40.

best value of R_m consistent with all experiments. There is no such convenient parameter presently available for inelastic scattering experiments.

The second factor affecting this analysis is the lack of restrictions on acceptable nuclear models used in analysis. From earlier theoretical considerations, a peaking at the nuclear surface is expected to be the dominant feature of the transition charge density. To determine the shape more fully, a probe with a shorter de Broglie wavelength is required. This indicates the need for electron-scattering experiments at higher energies, which have not yet been done for the states in question. Because these experiments are lacking, there is no *a priori* limitation on the shape of the transition charge used in analysis. As far as low-energy scattering is concerned, almost any model which incorporates a surface peaking could be used and presumably would give results similar [for the same $B(EL\uparrow)$ and R_{tr}^2] with those stated here. However, given the nature of the distorted-wave calculation, a quantitative estimate of the degree of model independence must await a numerical exploration using various models for ρ_{tr}. In any case, the present data should form a valuable link between measurements of $B(EL)$ using γ rays ($q\approx 0$ experiment) and the high-q measurements needed to define ρ_{tr} more completely.

D. Comparison with Other Experiments

Table VII contains a list of the transition rates obtained in this work, as well as those obtained for the same states in other recent determinations. Also included are the most recent theoretical predictions of Gerace and Green,[8] who have calculated both the even- and odd-parity states for Ca^{40}. The calculations of Bertsch[9] are not as complete, but give a closer result for one of the transitions and are included for comparison.

The basis of all these calculations is the shell model, with intrinsic deformed states added, in an attempt to account for the large transition rates observed experimentally, as well as for the large number of low-lying energy levels in Ca^{40}. Bertsch includes only two-particle–two-hole (2p-2h) deformed states in his calculation of the even-parity states. Gerace and Green have included not only 2p-2h but 4p-4h and 8p-8h states as well. In addition, they include the effects of a polarized core. For the odd-parity states, the usual 1p-1h calculation is extended by adding a 3p-3h deformed band.

Figure 1 shows levels observed in this and other experiments. The positive parity 4p-4h band of Gerace and Green corresponds to the observed states at 3.35 MeV (0+), 3.90 MeV (2+), and 5.27 MeV (4+). The 2p-2h band is not well established yet. The negative-parity band is not well founded either, but is based on the 5.90 MeV (1−) state. Their calculation gives 3− states at 3.8, 6.6, and 6.9 MeV, which correspond roughly to observed levels. The present work reports the sighting of another 3− state in this region.

In comparing with previous measurements, one should expect good agreement with those experiments which rely on the electromagnetic interaction for their interpretation, such as resonance fluorescence and Doppler-shift attenuation methods. Unfortunately, recent Doppler-shift measurements of the lifetimes of the Ca^{40} 3.90-MeV level are contradictory. As shown in Table VII, our result is in excellent agreement

with the $Ca^{40}(p, p'\gamma)Ca^{40}$ experiment,[35] but disagrees with two $K^{39}(p, \gamma)Ca^{40}$ measurements.[36,37] These latter agree with the older electron scattering work of Blum, Barreau, and Bellicard.[38] Although performed in the same momentum transfer range, interpretation of the 3.90-MeV peak in Ref. 38 is hampered by poorer experimental resolution; in addition, these results were analyzed using the Born-approximation formalism, which is expected[39] to overestimate $B(E2\uparrow)$. The discrepancy calls for further study; but in these circumstances it is reassuring to find that the present value for $B(E2\uparrow)$ of the 6.91-MeV Ca^{40} state is in excellent agreement with that derived from the resonance fluorescence study of Metzger,[40] as described in more detail below.

The heavy particle reaction cross sections have been related to the electromagnetic transition rates through the collective model, using the formula

$$B(EL\uparrow)=[(3/4\pi)ZeR_0^L]^2\beta_L^2,$$

where β_L is the deformation parameter which measures the amplitude of vibration about the spherical equilibrium shape of the nucleus. However, the equivalence is model-dependent, since these reactions are complicated by the appearance of specifically nuclear forces. This is particularly true of the α scattering since these particles are so strongly absorbed at the nuclear surface. Lippincott and Bernstein[4] in their recent work have attempted to deal with this question by enhancing their derived $B(EL)$ values by the ratio $(R_\alpha/R_{\rm EM})^2$, which explicitly differentiates between the radius of strong interaction for α particles and the radius for electromagnetic interaction. In any case, a difference between strengths measured in inelastic scattering of heavy particles and electrons may only signify that the two experiments are not, in fact, measuring the same quantity.

The results of the Yale work indicate that the first 2+ states of Ca^{40} (3.90 MeV) and Ca^{48} (3.83 MeV) have nearly the same strength in terms of single-particle units. This disagrees with the (α, α')[4,41] experiment, which finds the 2+ state of Ca^{48} almost twice as large. However, neither level is very collective in nature, involving at most five single-particle units. It is interesting that the theoretical predictions of Gerace and Green[8] are only able to give half the presently observed strength to the state in Ca^{40} while Bertsch's results[9] are in good agreement.

The first 3− states of these two isotopes have quite different strengths. The 3.73-MeV state of Ca^{40} is highly collective, with a strength of 32 single-particle units (spu). This strength agrees with that measured in inelastic α scattering,[4,41] in inelastic proton scattering,[42] and with the theoretical predictions of Gerace and Green.[8] Further, the present experiment confirms the result of Lippincott and Bernstein[4,41] that the first 3− state in Ca^{48} is much less strong than the corresponding state in Ca^{40}. This decrease in strength may be in part due to the blocking effect that the $f_{7/2}$ neutrons of Ca^{48} have on available particle-hole states.

Earlier evidence for a complex of states near 6.94 MeV in Ca^{40} has come from the previous (ee') experiment,[38] (α, α') experiment,[4,43] and from (pp') results.[42,44] Grace and Poletti in a (pp') experiment[5] resolved the complex into three states at 6.91 MeV (2+), 6.93 MeV (?), and 6.95 MeV (1−), too close to be resolved in the Yale (e, e') experiments. The multipolarities in parentheses are based on the resonance fluorescence experiments of Metzger,[40] who finds no evidence for the 6.93-MeV state observed in the (p, p') experiments. The widths he obtains for γ decay to the ground-state yield $B(EL\uparrow)$ values which are

$$B(E2\uparrow)=71\pm10e^2\ \mathrm{F}^4, \qquad B(E1\uparrow)=0.04e^2\ \mathrm{F}^2.$$

The $B(E1)$ value is much too small to be observed in our (e, e') experiment, and so the experimental form factor was analyzed as though the 1− were not present. Using values $c_{\rm tr}$ and $t_{\rm tr}$ equal to the ground-state values, a 2+ form factor alone would not fit the data. Using these same values for $c_{\rm tr}$ and $t_{\rm tr}$, a combination of 2+ and 3− was tried, yielding a good fit (Fig. 10) with a $B(E2\uparrow)$ of $70\pm10e^2$ F^4 and a $B(E3\uparrow)$ of $9200e^2$ F^6. The $B(E2\uparrow)$ is in excellent agreement with Metzger, and permits us to identify the 2+ component of this unresolved peak with the 6.91-MeV state. The 3− component must be identified with the 6.93-MeV level. However, this 3− assignment conflicts with the results of Lippincott and Bernstein,[4] who claim only a 1− state in addition to the 2+. However, since a 1− and 3− angular distribution are almost identical for (α, α') experiments except at very forward angles, it would seem their results could admit to a 3− state being present.

The surprising feature of this new 3− state is its strength, being half the size of the first excited 3− state, and several times larger than the 3− states at 6.29 and 6.58 MeV. These were only barely seen in this experiment (with approximate strengths of 2 and 3 spu, respectively) but are quite noticeable in

[35] J. R. MacDonald, D. F. H. Start, R. Anderson, A. G. Robertson, and M. A. Grace, Nucl. Phys. **A108**, 6 (1968).
[36] H. Lindeman, G. A. P. Engelbertink, M. W. Ockeloen, and H. S. Pruys, Nucl. Phys. **A122**, 373 (1968).
[37] K. W. Dolan and D. K. McDaniels, Phys. Rev. **175**, 1446 (1968).
[38] D. Blum, P. Barreau, and J. Bellicard, Phys. Letters **4**, 109 (1963).
[39] D. S. Onley, J. T. Reynolds, and L. E. Wright, Phys. Rev. **134**, B945 (1964).
[40] F. R. Metzger, Phys. Rev. **165**, 1245 (1968).
[41] A. M. Bernstein (private communication).
[42] W. S. Gray, R. A. Kenefick, and J. J. Kraushaar, Nucl. Phys. **67**, 542 (1965).
[43] A. Springer and B. G. Harvey, Phys. Letters **14**, 116 (1965).
[44] K. Yagi, H. Ejiri, M. Furukawa, Y. Ishizaki, M. Koike, K. Matsuda, Y. Nakajima, I. Nonaka, Y. Saji, E. Tanaka, and G. R. Satchler, Phys. Letters **10**, 186 (1964).

TABLE VIII. Comparison of total strengths measured in this experiment to those predicted on the basis of the energy-weighted sum rule (EWSR) and the shell-model sum rule (SMSR). See the text.

Nucleus	Level (MeV)	$B(E2\uparrow)$ (e^2 F^4)	$\frac{B(E2\uparrow)}{\text{SMSR}}$	$\frac{B(E2\uparrow)}{\text{EWSR}}$
		*E*2 Excitations		
Ca^{40}	3.90	84	0.050	0.033
	6.91	70	0.042	0.050
			0.092	0.083 sum
Ca^{48}	3.83	86	0.056	0.041
		*E*3 Excitations		
Nucleus	Level (MeV)	$B(E3\uparrow)$ (e^2 F^6)	$\frac{B(E3\uparrow)}{\text{SMSR}}$	$\frac{B(E3\uparrow)}{\text{EWSR}}$
Ca^{40}	3.73	21 000	0.367	0.153
	6.93	9 200	0.160	0.124
			0.527	0.277 sum
Ca^{48}	4.51	6 500	0.135	0.075

the (α, α') of Lippincott and Bernstein, where they have strengths[41] of 6.6 ± 1.0 and 3.8 ± 0.6 spu, respectively. Theoretical predictions of Gerace and Green show a state at 6.93 MeV, although its strength is only 3 spu as opposed to 14 spu observed here experimentally.

In Ca^{48}, weak octupole states at 5.37 and 7.68 MeV were observed. No attempt was made to study them in detail, but their strengths relative to the 4.51-MeV state allow assignment of approximate values for $B(E3\uparrow)$ of ~0.2 and ~1.5 spu, respectively.

Two sum rules have been derived which can give an estimate of the total transition strength of a given multipolarity within a nucleus. The first is the shell-model sum rule[45] (SMSR) which states that

$$\sum_f B(EL, i\to f) = \frac{(2L+1)Ze^2\langle r^{2L}\rangle}{4\pi}.$$

The sum extends over states of all energies up to the meson threshold. $\langle r^{2L}\rangle$ is the $2L$th moment of the ground-state distribution stated earlier. This shell-model sum provides an underestimate, since no coherent correlations are included. The second is the energy-weighted sum rule (EWSR),[46] which takes the following form for $T=0$ excitations:

$$\sum_f (E_f-E_i)B(EL, i\to f) = \frac{Z^2e^2L(2L+1)^2\langle r^{2L-2}\rangle}{8\pi AM}.$$

This rule is valid in general, unless there are velocity-dependent forces in the nuclear Hamiltonian.

Table VIII shows the transition strengths determined in this experiment relative to these sum rules. It is noteworthy that each of the 2+ states investigated in this work exhausts only $\sim5\%$ of the sum rules, suggesting that there must be other 2+ strength scattered throughout both Ca^{40} and Ca^{48}. There are several 2+ states reported for Ca^{40}, for example, in the (α, α')[4] work, and altogether these states exhaust $\sim20\%$ of SMSR and EWSR. There seems to be no larger, really collective, 2+ state in these nuclei. However, Ca^{42} and Ca^{44} seem to have such a state; lying at ~1.3 MeV, they are 10 spu each.

The two 3− states of Ca^{40} observed in detail by this experiment are both collective in nature. Together, they exhaust 53% of SMSR and 28% of EWSR. Including the states at 6.29 and 6.58 MeV (with strengths by Lippincott and Bernstein[4]) increases SMSR to $\sim70\%$ and EWSR to $\sim38\%$. The state in Ca^{48} is not nearly so strong, filling out only 13% of SMSR and 8% of EWSR. Including the other two states in Ca^{48} observed by Lippincott and Bernstein at 5.37 and 7.68 MeV moves these to $\sim22\%$ for SMSR and $\sim15\%$ for EWSR.

One may conclude that the largest part of the octupole strength in Ca^{40} is concentrated at low excitation (<8 MeV), supporting its description as an easily deformed nucleus. On the other hand, Ca^{48} appears more rigid, as befits an honest doubly magic nucleus.

ACKNOWLEDGMENTS

The authors are indebted to Dr. J. R. Stewart, for help in data accumulation, and to Dr. R. J. Peterson for valuable discussions. P. Jewett and W. Knudsen and the accelerator crew are responsible for stable machine operation. We thank also Professor H. L. Schultz for his interest and encouragement. The cooperation of Dr. George Rogosa in arranging a loan of the Ca^{48} material is greatly appreciated.

[45] A. M. Lane and E. D. Pendlebury, Nucl. Phys. 15, 39 (1960).

[46] O. Nathan and S. Nilsson, in *Alpha-, Beta-, and Gamma-Ray Spectroscopy*, edited by Kai Siegbahn (North-Holland Publishing Co., Amsterdam, 1965), Chap. X.